Received: Added at production | Revised: Added at production | Accepted: Added at production

DOI: xxx/xxxx

RESEARCH ARTICLE

A new non-stationary preconditioned iterative method for linear discrete ill-posed problems with application to image deblurring

Alessandro Buccini*[1] | Marco Donatelli[2] | Lothar Reichel[3] | Wei-Hong Zhang[4]

[1]Department of Matematics and Computer Sciences, University of Cagliari, 09124 Cagliari, Italy
[2]Department of Science and High Technology, University of Insubria, 22100 Como, Italy
[3]Department of Mathematical Sciences, Kent State University, Kent, OH, 44242, USA
[4]School of Mathematics and Statistics, Lanzhou University, Lanzhou 730000, Gansu Province, P. R. China

Correspondence
*Alessandro Buccini, Via Ospedale 72, 09124 Cagliari, Italy. Email: alessandro.buccini@unica.it

Summary

Discrete ill-posed inverse problems arise in many areas of science and engineering. Their solutions are very sensitive to perturbations in the data. Regularization methods aim at reducing this sensitivity. This paper considers an iterative regularization method, based on iterated Tikhonov regularization, that was proposed in [M. Donatelli and M. Hanke, Fast nonstationary preconditioned iterative methods for ill-posed problems, with application to image deblurring, Inverse Problems, 29 (2013), Art. 095008, 16 pages]. In this method, the exact operator is approximated by an operator that is easier to work with. However, the convergence theory requires the approximating operator to be spectrally equivalent to the original operator. This condition is rarely satisfied in practice. Nevertheless, this iterative method determines accurate image restorations in many situations. We propose a modification of the iterative method, that relaxes the demand of spectral equivalence to a requirement that is easier to satisfy. We show that, although the modified method is not an iterative regularization method, it maintains one of the most important theoretical properties for this kind of methods, namely monotonic decrease of the reconstruction error. Several computed experiments show the good performances of the proposed method.

KEYWORDS:
discrete ill-posed inverse problems, iterated Tikhonov method, spectral equivalence

1 | INTRODUCTION

We are concerned with the solution of discrete ill-posed problems of the form

$$\min_{\mathbf{x}\in\mathbb{R}^n} \|A\mathbf{x} - \mathbf{b}^\delta\|, \tag{1}$$

where $A \in \mathbb{R}^{m\times n}$ is a matrix, whose singular values decay to zero with increasing index, without a significant gap. In particular, the matrix A is of ill-determined rank and may be rank-deficient; see, e.g., [1, 2] for discussions on ill-posed and discrete ill-posed problems. The norm $\|\cdot\|$ in (1) denotes the Euclidean vector norm. The vector $\mathbf{b}^\delta \in \mathbb{R}^m$ represents measured data and is corrupted by an error $\boldsymbol{\eta} \in \mathbb{R}^m$, i.e., $\mathbf{b}^\delta = \mathbf{b} + \boldsymbol{\eta}$, where $\mathbf{b} \in \mathbb{R}^m$ is the unavailable error-free vector associated with $\mathbf{b}^\delta$. We will assume that each entry of $\boldsymbol{\eta}$ is the realization of a Gaussian random variable with zero mean, and we sometimes will refer to the error $\boldsymbol{\eta}$ as "noise".

Let $A^\dagger$ denote the Moore-Penrose pseudo-inverse of A. Due to the presence of the error $\boldsymbol{\eta}$ in $\mathbf{b}^\delta$ and the ill-conditioning of A, the naïve solution $A^\dagger\mathbf{b}^\delta$ of (1) is usually a poor approximation of the desired vector $\mathbf{x}_{\text{true}} = A^\dagger\mathbf{b}$. To reduce the sensitivity of the

vector $A^\dagger \mathbf{b}^\delta$ to the error $\boldsymbol{\eta}$, one generally applies a regularization method to compute an approximate solution of (1). One of the most popular regularization methods is Tikhonov regularization, which replaces (1) by the penalized least-squares problem

$$\mathbf{x}_\mu = \arg\min_{\mathbf{x}\in\mathbb{R}^n} \{ \|A\mathbf{x} - \mathbf{b}^\delta\|^2 + \mu \|\mathbf{x}\|^2 \}, \tag{2}$$

where $\mu > 0$ is a regularization parameter. We note for future reference that the solution of (2) can be written as

$$\mathbf{x}_\mu = (A^T A + \mu I)^{-1} A^T \mathbf{b}^\delta = A^T (AA^T + \mu I)^{-1} \mathbf{b}^\delta, \tag{3}$$

where the superscript ^{T} denotes transposition.

The sensitivity of the solution $\mathbf{x}_\mu$ of (2) to the error $\boldsymbol{\eta}$ and the closeness of $\mathbf{x}_\mu$ to the desired solution $\mathbf{x}_{\text{true}}$ depends on the choice of the regularization parameter μ. We will assume that a fairly accurate estimate δ for $\|\boldsymbol{\eta}\|$ is known, i.e.,

$$\|\mathbf{b}^\delta - \mathbf{b}\| \leq \delta, \tag{4}$$

and that $\mathbf{b}$ is in the range of A. Then μ can be determined by the discrepancy principle, which prescribes that $\mu > 0$ be chosen so that

$$\|A\mathbf{x}_\mu - \mathbf{b}^\delta\| = \tau\delta,$$

where $\tau > 1$ is a user-specified constant that is independent of δ; see, e.g., [1]. Other methods for determining μ also can be used, including the L-curve criterion and generalized cross validation; see [2–6] for discussions.

Many strategies have been proposed for improving the accuracy of the computed solution (3), i.e., its closeness to the desired solution $\mathbf{x}^\dagger$, such as imposing nonnegativity constraints [7–10], inserting a regularization operator L in the second term of (2) [11–14], and by iterative improvement [15–19]. In this paper we consider the latter approach.

Let $\mathbf{x}_k$ be an approximate solution of (1) and define the error

$$\mathbf{e}_k = \mathbf{x}_{\text{true}} - \mathbf{x}_k. \tag{5}$$

An approximation $\mathbf{h}_k$ of $\mathbf{e}_k$ can be determined by solving the least-squares problem

$$\min_{\mathbf{h}\in\mathbb{R}^n} \|A\mathbf{h} - \mathbf{r}_k\|, \tag{6}$$

where $\mathbf{r}_k = \mathbf{b}^\delta - A\mathbf{x}_k$. Since A is ill-conditioned and $\mathbf{r}_k$ is contaminated by error, an approximate solution of (6) can be obtained by Tikhonov regularization (2). Thus, we can solve

$$\mathbf{h}_k = A^T (AA^T + \mu I)^{-1} \mathbf{r}_k.$$

An improved approximation of $\mathbf{x}^\dagger$ may then be computed as

$$\mathbf{x}_{k+1} = \mathbf{x}_k + \mathbf{h}_k = \mathbf{x}_k + A^T (AA^T + \mu I)^{-1} \mathbf{r}_k. \tag{7}$$

This iterative method can be seen as a preconditioned version of Landweber iteration with preconditioner $A^T(AA^T + \mu I)^{-1}$, and is commonly referred to as the iterated Tikhonov method; see [1, 15] for more details. We remark that although it would be natural to regard $(AA^T + \mu I)^{-1}$ as the preconditioner, we will refer to $A^T(AA^T + \mu I)^{-1}$ as the preconditioner, following the notation of [16]. The main drawbacks of the iterative method (7) are that i) when the matrix A is large, a large linear system of equations has to be solved at each iteration, and ii) the computed solution may be sensitive to the choice of the parameter μ. Donatelli and Hanke address these difficulties in [16] by replacing the matrix A in the preconditioner $A^T(AA^T + \mu I)^{-1}$ by a matrix C, whose structure allows fast application of the preconditioner, and by choosing the parameter μ so that it satisfies a damped version of the discrepancy principle. This algorithm, which is described below by Algorithm 1, is demonstrated in [16] to give accurate image reconstructions for a reasonable computational cost for several examples. Following, Donatelli and Hanke [16], we refer to their method as the Approximated Iterated Tikhonov (AIT) method. This algorithm (or similar variants) are also discussed in [18, 20–23].

Donatelli and Hanke [16] provide a theoretical analysis of the AIT method. In particular, they show that it is a regularization method under the assumption that the matrices A and C are spectrally equivalent; see Assumption 1 below. Unfortunately, this requirement is rarely satisfied in practical applications. Nevertheless, Algorithm 1 performs well when applied to image reconstruction problems with sufficiently much noise in the data vector $\mathbf{b}^\delta$.

It is the purpose of the present paper to weaken the spectrally equivalence assumption and to propose a new iterative method, which we will refer to as the Modified Approximated Iterated Tikhonov (MAIT) method. We will show convergence results for this method. Numerical examples reported in Section 4 illustrate that when the error in $\mathbf{b}^\delta$ is large enough, the MAIT and AIT methods determine very similar image reconstructions. On the other hand, when the error in $\mathbf{b}^\delta$ is small, the AIT method may fail, while the MAIT method is able to provide accurate reconstructions. We remark that our requirement on A and C is weaker

than spectral equivalence, however the MAIT method is not a regularization method. We recall that an algorithm is said to be a regularization method if, denoting by $\mathbf{x}^\delta$ the approximate solution computed with right-hand side $\mathbf{b}^\delta$, it holds that $\mathbf{x}^\delta \to \mathbf{x}^\dagger$ as $\delta \to 0$; see [1] for more details on regularization methods. Nevertheless, we are able to provide some theoretical insight on the performance of the MAIT method.

In this paper we consider, similarly as in [16], image deblurring as our main application, since, as we will illustrate in Section 4, in this application it is straightforward to find a matrix C that is easy to work with and approximates A well. However, our method also can be applied to other large-scale discrete ill-posed problems for which the given matrix A can be approximated well by a "simpler matrix" C.

This paper is structured as follows: Section 2 describes the AIT method by Donatelli and Hanke [16] and recalls the theoretical results available for this method. We describe our modified method in Section 3, where we also present some analysis of the method. Section 4 reports numerical results, and concluding remarks can be found in Section 5.

2 | THE APPROXIMATED ITERATED TIKHONOV METHOD

We outline the AIT method and discuss the main theoretical results shown by Donatelli and Hanke [16]. In particular, Donatelli and Hanke [16] make the following assumption.

Assumption 1. (Spectral equivalence) Let $A, C \in \mathbb{R}^{m\times n}$ and $0 < \rho < 1/2$. Assume that, for all $\mathbf{z} \in \mathbb{R}^n$, it holds

$$\|(A - C)\mathbf{z}\| \leq \rho \|A\mathbf{z}\|.$$

It is easy to see that Assumption 1 implies that $\mathcal{N}(A) = \mathcal{N}(C)$, where $\mathcal{N}(M)$ denotes the null space of the matrix M.

Algorithm 1 AIT

Let A and C satisfy Assumption 1 for a given $0 < \rho < 1/2$, and fix $q \in (2\rho, 1)$. Let $\delta > 0$ satisfy (4) and let $\mathbf{x}_0$ be an initial guess for $\mathbf{x}^\dagger$.

$\mathbf{r}_0 = \mathbf{b}^\delta - A\mathbf{x}_0$
$\tau = \frac{1+2\rho}{1-2\rho}$
for $k = 0, 1, \ldots$ **do**
  $\tau_k = \left\|\mathbf{r}_k\right\| / \delta$
  $q_k = \max\{q, 2\rho + (1+\rho)/\tau_k\}$
  Determine μ_k such that $\left\|\mathbf{r}_k - CC^T(CC^T + \mu_k I)^{-1}\mathbf{r}_k\right\| = q_k \left\|\mathbf{r}_k\right\|$
  $\mathbf{h}_k = C^T(CC^T + \mu_k I)^{-1}\mathbf{r}_k$
  $\mathbf{x}_{k+1} = \mathbf{x}_k + \mathbf{h}_k$
  $\mathbf{r}_{k+1} = \mathbf{b}^\delta - A\mathbf{x}_{k+1}$
  if $\left\|\mathbf{r}_{k+1}\right\| \leq \tau\delta$ **then**
    exit
  end if
end for

We review some results shown by Donatelli and Hanke [16] about the AIT method.

Proposition 1. (Reference [16]) Let Assumption 1 hold and let $\tau_* = (1+\rho)/(1-2\rho)$. Then, if $\tau_k = \left\|\mathbf{r}_k\right\| / \delta > \tau_*$, it follows that

$$\|\mathbf{r}_k - C\mathbf{e}_k\| \leq \left(\rho + \frac{1+\rho}{\tau_k}\right) \left\|\mathbf{r}_k\right\| < (1-\rho) \left\|\mathbf{r}_k\right\|,$$

where $\mathbf{e}_k = \mathbf{x}^\dagger - \mathbf{x}_k$ and $\mathbf{r}_k = \mathbf{b}^\delta - A\mathbf{x}_k$.

The following result shows that the norm of the error $\mathbf{e}_k$ in the iterates $\mathbf{x}_k$, cf. (5), decreases monotonically with the iteration number, k, until the discrepancy principle is satisfied.

Proposition 2. (Reference [16]) Let Assumption 1 hold. Then the norm of the error $\mathbf{e}_k$ in the iterate $\mathbf{x}_k$ generated by Algorithm 1 decreases monotonically,

$$\|\mathbf{e}_k\|^2 - \|\mathbf{e}_{k+1}\|^2 \geq 2\rho \|(CC^T + \mu_k I)^{-1}\mathbf{r}_k\| \, \|\mathbf{r}_k\|,$$

as long as $\|\mathbf{r}_k\| > \tau\delta$, where $\mathbf{r}_k = \mathbf{b}^\delta - A\mathbf{x}_k$.

Corollary 1. (Reference [16]) Under the assumptions of Proposition 2, let k_δ denote index of the last iterate determined by Algorithm 1. Then

$$\|\mathbf{e}_0\|^2 \geq 2\rho \sum_{k=0}^{k_\delta - 1} \|(CC^T + \mu_k I)^{-1}\mathbf{r}_k\| \, \|\mathbf{r}_k\| \geq c \sum_{k=0}^{k_\delta - 1} \left\|\mathbf{r}_k\right\|^2,$$

for some constant $c > 0$ that only depends on ρ and q, where q is defined in Algorithm 1.

The above corollary implies that, if $\delta > 0$, then the computations with Algorithm 1 terminate after a finite number of iterations. The following theorem shows that, when $\delta = 0$, the iterates generated by Algorithm 1 converge to a solution of the exact problem (with data vector $\mathbf{b}$) that is closest to $\mathbf{x}_0$. In particular, if $\mathbf{x}_0 = \mathbf{0}$ and $\delta = 0$, then the iterations of Algorithm 1 converge to $\mathbf{x}_{\text{true}}$.

Theorem 1. (Reference [16]) Assume that $\delta = 0$ and that $\mathbf{x}_0$ is not a solution of (1) with $\mathbf{b}^\delta$ replaced by $\mathbf{b}$. Then the sequence of iterates $\mathbf{x}_k$, $k = 0, 1, 2, \ldots$, generated by Algorithm 1 converges as $k \to \infty$ to the solution of (1) that is closest to $\mathbf{x}_0$.

The AIT algorithm is an iterative regularization method, i.e., the following result holds.

Theorem 2. (Reference [16]) Let Assumption 1 be valid and let $\delta \mapsto \mathbf{b}^\delta$ be a function such that (4) holds for all $\delta > 0$. For fixed parameters τ and q (defined in Algorithm 1), let $\mathbf{x}^\delta$ denote the approximate solution computed by Algorithm 1. Then, as $\delta \to 0$, $\mathbf{x}^\delta$ converges to the solution of (1) that is closest to $\mathbf{x}_0$.

3 | A MODIFIED APPROXIMATED ITERATED TIKHONOV METHOD

This section describes an alternative to Algorithm 1, whose analysis does not require Assumption 1. We first relax this assumption as follows.

Assumption 2. (Relaxed spectral equivalence) Let $A, C \in \mathbb{R}^{m\times n}$, $\beta \geq 0$, and $0 < \rho < 1/2$. Assume that, for all $\mathbf{z} \in \mathbb{R}^n$, it holds

$$\|(A - C)\mathbf{z}\| \leq \rho(\|A\mathbf{z}\| + \beta).$$

Let us first observe that if $\beta = 0$, then the Assumptions 1 and 2 are exactly the same. For a general $\beta > 0$, we have that Assumption 1 implies Assumption 2, but the converse is not true. Here β plays the role of a "relaxation parameter" as, intuitively, it measures how much weaker Assumption 2 is than Assumption 1. In particular, the larger β is, the easier it is to satisfy Assumption 2. The latter assumption forms the basis for Algorithm 2.

Algorithm 2 differs from Algorithm 1 in the definition of τ_k and in the stopping criterion. The introduction of the parameter t_0 is technical and will help in the following proofs. Intuitively, this parameter measures the relative importance of β and δ. We would like to briefly discuss the stopping criterion of Algorithm 2. Let us first observe the following:

Lemma 1. With the notation and assumptions of Algorithm 2, assume that $\|\mathbf{r}_k\| > 0$ and that C is not the zero matrix. Then the equation

$$\|\mathbf{r}_k - CC^T(CC^T + \mu_k I)^{-1}\mathbf{r}_k\| = q_k\|\mathbf{r}_k\| \tag{8}$$

has a unique solution $0 < \mu_k < \infty$ when $0 < q_k < 1$ is close enough to 1, and the components of $\mathbf{r}_k$, when expressed in terms of the eigenvectors of CC^T, satisfy the conditions (11) specified in the proof. These conditions are generally satisfied.

Proof. Assume first that $q_k = 0$ and $\mu_k > 0$. Then it follows from (8) that $\mathbf{r}_k = CC^T(CC^T + \mu_k I)^{-1}\mathbf{r}_k$, which is equivalent to $\mathbf{r}_k = (CC^T + \mu_k I)^{-1}CC^T\mathbf{r}_k$. This equation only holds if $\mu_k\mathbf{r}_k = \mathbf{0}$. Hence, $q_k > 0$.

The symmetric positive semidefinite matrix CC^T has a spectral decomposition $CC^T = Q\Lambda Q^T$, where the matrix $Q \in \mathbb{R}^{m\times m}$ is orthogonal and $\Lambda = \text{diag}[\lambda_1, \lambda_2, \ldots, \lambda_m]$ contains the nonnegative eigenvalues. Substituting this decomposition into (8) and squaring the equation gives

$$\|\mathbf{r}_k - Q\Lambda(\Lambda + \mu_k I)^{-1}Q^T\mathbf{r}_k\|^2 = q_k^2\|\mathbf{r}_k\|^2. \tag{9}$$

Let $\hat{\mathbf{r}} = [\hat{r}_1, \hat{r}_2, \ldots, \hat{r}_m]^T = Q^T\mathbf{r}_k$ and define the index sets

$$J = \{j : 1 \leq j \leq m, \hat{r}_j \neq 0\}, \quad J_1 = \{j \in J : \lambda_j \neq 0\}, \quad J_0 = J \setminus J_1 = \{j \in J : \lambda_j = 0\}.$$

Algorithm 2 MAIT

Let A and C satisfy Assumption 2 for given $0 < \rho < 1/2$ and $\beta \geq 0$. Fix $q \in (2\rho, 1)$, let $\delta > 0$ satisfy (4), and let $\mathbf{x}_0$ be an initial approximation of $\mathbf{x}^\dagger$.

$t_0 = \min\left\{\frac{\delta}{\beta}, \frac{\beta}{\delta}\right\} + 1$
$\mathbf{r}_0 = \mathbf{b}^\delta - A\mathbf{x}_0$
$\tau = \frac{1+2\rho}{1-2\rho}$
for $k = 0, 1, \ldots$ **do**
  $\tau_k = t_0 \dfrac{\|\mathbf{r}_k\|}{\delta + \beta}$
  $q_k = \max\{q, 2\rho + (1+\rho)/\tau_k\}$
  Determine μ_k such that $\|\mathbf{r}_k - CC^T(CC^T + \mu_k I)^{-1}\mathbf{r}_k\| = q_k\|\mathbf{r}_k\|$
  $\mathbf{h}_k = C^T(CC^T + \mu_k I)^{-1}\mathbf{r}_k$
  $\mathbf{x}_{k+1} = \mathbf{x}_k + \mathbf{h}_k$
  $\mathbf{r}_{k+1} = \mathbf{b}^\delta - A\mathbf{x}_{k+1}$
  if $\|\mathbf{r}_{k+1}\| \leq \tau\delta$ or $\|\mathbf{r}_{k+1}\| \leq \tau\dfrac{\delta+\beta}{t_0}$ **then**
    exit
  end if
end for

Then (9) can be expressed as

$$\sum_{j\in J_1}\left(1 - \frac{\lambda_j}{\lambda_j + \mu_k}\right)^2 \hat{r}_j^2 + \sum_{j\in J_0}\hat{r}_j^2 = \sum_{j\in J} q_k^2 \hat{r}_j^2. \tag{10}$$

Introduce the function

$$\phi(\mu) = \sum_{j\in J_1}\left(1 - \frac{\lambda_j}{\lambda_j + \mu}\right)^2 \hat{r}_j^2.$$

Then

$$\phi(0) = 0, \quad \lim_{\mu\to\infty}\phi(\mu) = \sum_{j\in J_1}\hat{r}_j^2,$$

and the derivative satisfies $\phi'(0) = 0$ and $\phi'(\mu) > 0$ for $\mu > 0$. Hence, the function $\phi(\mu)$ is monotonically increasing for $\mu > 0$. It follows that equation (10) has a unique finite solution $\mu = \mu_k$ if and only if

$$\sum_{j\in J_0}\hat{r}_j^2 < q_k^2\sum_{j\in J}\hat{r}_j^2 \quad \text{and} \quad \sum_{j\in J}\hat{r}_j^2 > q_k^2\sum_{j\in J}\hat{r}_j^2. \tag{11}$$

The right-hand side inequality holds when $0 < q_k < 1$ and the left-hand side inequality holds when q_k is large enough and the cardinality of J_0 is small enough compared to the cardinality of J. □

Remark 1. Observe that, by construction, $q \leq q_k$. Therefore, the conditions in Lemma 1 on q_k can be satisfied by choosing q large enough. We set $q = 0.7$ in the numerical experiments reported in Section 4.

Lemma 1 is relevant for both Algorithms 1 and 2. We now derive a condition that secures that $0 \leq q_k < 1$. First consider Algorithm 2. By the proof of Lemma 1, we have $q_k > 0$. We therefore only need to check under which condition $q_k < 1$. By the definitions of q_k and τ_k, we have

$$q_k = \max\left\{q, 2\rho + \frac{1+\rho}{\tau_k} = 2\rho + \frac{(1+\rho)(\delta+\beta)}{t_0\|\mathbf{r}_k\|}\right\}.$$

Thus, since $q < 1$, $q_k < 1$ if and only if

$$2\rho + \frac{(1+\rho)(\delta+\beta)}{t_0\|\mathbf{r}_k\|} < 1,$$

which is equivalent to

$$\|\mathbf{r}_k\| > \frac{1+\rho}{1-2\rho}\frac{\delta+\beta}{t_0}. \tag{12}$$

Thus, the additional stopping criterion in Algorithms 2 is included to ensure that the computation of μ_k can be carried out since $\tau > \frac{1+\rho}{1-2\rho}$.

Observe that, when we let $\beta \to 0^+$, Algorithm 2 reduces to Algorithm 1, since $t_0 \to 1$. Thus, condition (12) for AIT translates into

$$\|\mathbf{r}_k\| > \frac{1+\rho}{1-2\rho}\delta,$$

which is always satisfied if $\|\mathbf{r}_k\| > \frac{1+2\rho}{1-2\rho}\delta$. Thus, $q_k < 1$ for all k in Algorithm 1. Therefore, the algorithm does not need the additional stopping criterion of Algorithm 2.

Remark 2. We would like to discuss for which values of β the additional stopping criterion of Algorithm 2 does not terminate the iterations before the discrepancy principle is satisfied. In other words, we would like to solve the inequality

$$\tau\frac{\delta+\beta}{t_0} \le \tau\delta.$$

Simple computations show that, in order for the discrepancy principle to be satisfied, we need

$$\beta \le (t_0 - 1)\delta.$$

This means that the discrepancy principle can be satisfied only if the error in $\mathbf{b}^\delta$ is able to "cover" the approximation error β. In particular, this shows that when the data vector $\mathbf{b}^\delta$ is error-free, we cannot expect the iterates generated by Algorithm 2 to converge to an exact solution of the problem (1) if $\beta > 0$. It follows that the MAIT method is not a regularization method. Nevertheless, we will show below that the MAIT method has some desirable properties and is able to determine accurate image restorations.

The following auxiliary result is needed below.

Proposition 3. Assume that Assumption 2 holds, and let $\tau_k = t_0\frac{\|\mathbf{r}_k\|}{\delta+\beta}$, where $t_0 = \min\left\{\frac{\beta}{\delta}, \frac{\delta}{\beta}\right\} + 1$ is defined in Algorithm 2. Then

$$\|\mathbf{r}_k - C\mathbf{e}_k\| \le \left(\rho + t_0\frac{1+\rho}{\tau_k}\right)\|r_k\| - \beta.$$

Proof. We have

$$\begin{aligned}
\|\mathbf{r}_k - C\mathbf{e}_k\| &= \|\mathbf{b}^\delta - \mathbf{b} + \mathbf{b} - A\mathbf{x}_k - C\mathbf{e}_k\| \\
&= \|\mathbf{b}^\delta - \mathbf{b} + A(\mathbf{x}^\dagger - \mathbf{x}_k) - C\mathbf{e}_k\| \\
&\le \|\mathbf{b}^\delta - \mathbf{b}\| + \|(A - C)(\mathbf{x}^\dagger - \mathbf{x}_k)\| \\
&\le \|\mathbf{b}^\delta - \mathbf{b}\| + \rho(\|A(\mathbf{x}^\dagger - \mathbf{x}_k)\| + \beta) \\
&\le \|\mathbf{b}^\delta - \mathbf{b}\| + \rho(\|\mathbf{b} - \mathbf{b}^\delta + \mathbf{b}^\delta - A\mathbf{x}_k\| + \beta) \\
&\le (1+\rho)\delta + \rho\|\mathbf{r}_k\| + \rho\beta.
\end{aligned}$$

By the definition of τ_k, we get

$$\delta = t_0\frac{\|\mathbf{r}_k\|}{\tau_k} - \beta.$$

Substituting this expression into the above inequality yields

$$\|\mathbf{r}_k - C\mathbf{e}_k\| \le (1+\rho)\left(t_0\frac{\|\mathbf{r}_k\|}{\tau_k} - \beta\right) + \rho\|\mathbf{r}_k\| + \rho\beta = \left(\rho + t_0\frac{1+\rho}{\tau_k}\right)\|\mathbf{r}_k\| - \beta.$$

□

We can now show our main result.

Theorem 3. Let Assumption 2 hold. With the notation of Algorithm 2, we have that, if

$$\|\mathbf{r}_{k+1}\| > \tau\delta \quad \text{and} \quad \|\mathbf{r}_{k+1}\| > \tau\frac{\delta+\beta}{t_0},$$

then

$$\|\mathbf{e}_k\|^2 - \|\mathbf{e}_{k+1}\|^2 \ge 2\rho\frac{\tau-1}{\tau}\|(CC^T + \mu_k I)^{-1}\mathbf{r}_k\|\,\|\mathbf{r}_k\|.$$

In particular, it follows from $\tau > 1$, that $\|\mathbf{e}_k\|$ decreases monotonically as k increases.

Proof. The proof of this result is inspired by the proof of [16, Proposition 2]. Let $\langle \mathbf{v}, \mathbf{u} \rangle$ denote the standard inner product. Then we obtain

$$\begin{aligned}
\|\mathbf{e}_k\|^2 - \|\mathbf{e}_{k+1}\|^2 &= 2\langle \mathbf{e}_k, \mathbf{h}_k \rangle - \|\mathbf{h}_k\|^2 \\
&\geq 2\left\langle \mathbf{e}_k, C^T(CC^T + \mu_k I)^{-1}\mathbf{r}_k \right\rangle - 2\left\langle \mathbf{r}_k, CC^T(CC^T + \mu_k I)^{-2}\mathbf{r}_k \right\rangle \\
&= 2\left\langle \mathbf{r}_k, (CC^T + \mu_k I)^{-1}\mathbf{r}_k \right\rangle - 2\left\langle \mathbf{r}_k - C\mathbf{e}_k, (CC^T + \mu_k I)^{-1}\mathbf{r}_k \right\rangle \\
&\quad - 2\left\langle \mathbf{r}_k, CC^T(CC^T + \mu_k I)^{-2}\mathbf{r}_k \right\rangle \\
&= 2\left\langle \mathbf{r}_k, \mu_k(CC^T + \mu_k I)^{-2}\mathbf{r}_k \right\rangle - 2\left\langle \mathbf{r}_k - C\mathbf{e}_k, (CC^T + \mu_k I)^{-1}\mathbf{r}_k \right\rangle \\
&\geq 2\|(CC^T + \mu_k I)^{-1}\| \left(\|\mu_k(CC^T + \mu_k I)^{-1}\| - \|\mathbf{r}_k - C\mathbf{e}_k\| \right).
\end{aligned}$$

By the definition of $\mathbf{h}_k$, we have

$$\mathbf{r}_k - C\mathbf{h}_k = \mathbf{r}_k - CC^T(CC^T + \mu_k I)^{-1}\mathbf{r}_k = \mu_k(CC^T + \mu_k I)^{-1}\mathbf{r}_k.$$

Combining the above inequality and equality, and using the definitions of μ_k and τ_k, as well as Proposition 3, we obtain

$$\begin{aligned}
\|\mathbf{e}_k\|^2 - \|\mathbf{e}_{k+1}\|^2 &\geq 2\|(CC^T + \mu_k I)^{-1}\| \left(\|\mathbf{r}_k - C\mathbf{h}_k\| - \|\mathbf{r}_k - C\mathbf{e}_k\| \right) \\
&\geq 2\|(CC^T + \mu_k I)^{-1}\| \left(q_k\|\mathbf{r}_k\| - ((1+\rho)\delta + \rho\|\mathbf{r}_k\| + \rho\beta) \right) \\
&\geq 2\|(CC^T + \mu_k I)^{-1}\| \left(\left(2\rho + \frac{1+\rho}{\tau_k} - \rho \right) \|\mathbf{r}_k\| - (1+\rho)\delta - \rho\beta \right) \\
&\geq 2\|(CC^T + \mu_k I)^{-1}\| \left(\rho\|\mathbf{r}_k\| + \frac{1+\rho}{t_0\|\mathbf{r}_k\|}(\delta + \beta)\|\mathbf{r}_k\| - (1+\rho)\delta - \rho\beta \right) \\
&= 2\|(CC^T + \mu_k I)^{-1}\| \left(\rho\|\mathbf{r}_k\| + \frac{1+\rho}{t_0}(\delta + \beta) - (1+\rho)\delta - \rho\beta \right).
\end{aligned}$$

We now show that

$$\frac{1+\rho}{t_0}(\delta + \beta) - (1+\rho)\delta - \rho\beta \geq -\rho\delta.$$

First consider the expression

$$\frac{\delta + \beta}{t_0}.$$

If $\delta \geq \beta$, then $\delta/\beta \geq \beta/\delta$ and, thus,

$$\frac{\delta + \beta}{t_0} = \frac{\delta + \beta}{\beta/\delta + 1} = \delta. \tag{13}$$

Conversely, if $\delta \leq \beta$, then $\delta/\beta \leq \beta/\delta$ and, therefore,

$$\frac{\delta + \beta}{t_0} = \frac{\delta + \beta}{\delta/\beta + 1} = \beta. \tag{14}$$

Combining the expressions (13) and (14), we obtain

$$\frac{\delta + \beta}{t_0} = \max\{\beta, \delta\}.$$

We can now majorize

$$\frac{1+\rho}{t_0}(\delta + \beta) - (1+\rho)\delta - \rho\beta.$$

Thus,

$$\begin{aligned}
\frac{1+\rho}{t_0}(\delta + \beta) - (1+\rho)\delta - \rho\beta &= (1+\rho)\max\{\beta, \delta\} - (1+\rho)\delta - \rho\beta \\
&= (\max\{\beta, \delta\} - (1+\rho)\delta) + (\rho\max\{\beta, \delta\} - \rho\beta) \\
&\geq (\delta - (1+\rho)\delta) + (\rho\beta - \rho\beta) = -\rho\delta.
\end{aligned}$$

Recalling that, by assumption, $\|\mathbf{r}_k\| \geq \tau\delta$, we obtain

$$\begin{aligned}\|\mathbf{e}_k\|^2 - \|\mathbf{e}_{k+1}\|^2 &\geq 2\|(CC^T + \mu_k I)^{-1}\| \left(\rho\|\mathbf{r}_k\| - \rho\delta\right) \\ &\geq 2\|(CC^T + \mu_k I)^{-1}\| \left(\rho\|\mathbf{r}_k\| - \rho\frac{\|\mathbf{r}_k\|}{\tau}\right) \\ &= 2\|(CC^T + \mu_k I)^{-1}\|\rho\frac{\tau-1}{\tau}\|\mathbf{r}_k\|.\end{aligned}$$

□

4 | NUMERICAL EXAMPLES

We present a few numerical examples to illustrate the performance of the MAIT method. Like in [16, 17], we consider space-invariant image deblurring as our main application. Image blurring can be modeled by a Fredholm integral equation of the first kind,

$$b(s,t) = \int_\Omega \kappa(u,s,v,t)x(u,v)\mathrm{d}u\mathrm{d}v, \qquad (s,t) \in \Omega, \tag{15}$$

where b represents the blurred image, κ is a point spread function (PSF), and Ω is the domain of the exact image, which is represented by x. When the blur is spatially invariant, i.e., when the blur does not depend on the spacial location, we have $k(u,s,v,t) = k(u-s, v-t)$. This is the case in the computed examples below. Discretization of (15) gives a problem of the form (1), where the structure of the matrix $A \in \mathbb{R}^{n\times n}$ depends on the boundary conditions imposed; see, e.g., [24] for a discussion on image deblurring. For any of the standard boundary conditions commonly used, the matrix $A \in \mathbb{R}^{n\times n}$ can be written as

$$A = T + R + E,$$

where T is a block Toeplitz matrix with Toeplitz blocks, R is a matrix of low rank, and E is a matrix of small norm. The matrix A can be accurately approximated by a block circulant matrix C with circulant blocks associated to T; see, e.g., [12, 16, 24] for further details. The matrix C can be determined by imposing periodic boundary conditions when discretizing (15). We will choose this matrix in Assumption 2. This is the same choice as in [16]. The matrix C can be diagonalized by the discrete Fourier transform. Therefore, the vector $(CC^T + \mu_k I)^{-1}\mathbf{r}_k$ can be computed in $O(n\log n)$ arithmetic floating point operations with the aid of the fast Fourier transform algorithm. Moreover, the computation of μ_k in each iteration can be carried out cheaply with just a few iterations with Newton's method; see [16] for more details.

We set $\rho = 10^{-3}$ and $q = 0.7$ in all our computed examples, similarly as in [16]. In most of the computations, we set $\beta = 150$, however, we also will illustrate the effect of different choices of this parameter. Finally, we set the maximum number of iteration to 50 and, as suggested in [17], we set $\mathbf{x}_0 = A^T\mathbf{b}^\delta$. By Assumption 2, the choice of β is only required to depend on the matrices A and C. However, there is no easy way to determine which value to choose in actual computations. In the computed examples, we therefore choose β in an ad hoc manner.

To assess the quality of the computed solution, we compute the Relative Reconstruction Error (RRE), which is defined by

$$\mathrm{RRE}(\mathbf{x}) = \frac{\left\|\mathbf{x} - \mathbf{x}_{\mathrm{true}}\right\|}{\left\|\mathbf{x}_{\mathrm{true}}\right\|},$$

where $\mathbf{x}_{\mathrm{true}}$ represents the desired blur- and error-free image. Moreover, we also compute the Structure SIMilarity (SSIM) index defined in [25]. The definition of the SSIM index is quite involved and we do not report it here. Intuitively, the SSIM index measures how the computed image reconstructs the overall structure of the original image. The larger value of the SSIM index, the better the reconstruction. The largest possible value is 1.

We are primarily interested in illustrating how the MAIT and AIT methods compare. Therefore, we do not report results for other methods. Comparisons of the AIT and other image restoration methods are reported in [16, 17]. Our examples show the MAIT and AIT methods to perform very similarly when the latter converges, and that MAIT outperforms AIT when the latter fails to converge.

It is pointed out in [16] that the AIT method may fail if the amount of error that corrupts the data $\mathbf{b}^\delta$ is very small. This is due to the fact that in this case the error is not large enough to "cover" the approximation error made when approximating A by C when Assumption 1 does not hold. We will illustrate that when δ in (4) can be chosen small, the AIT method fails to converge, while the MAIT method produces an accurate reconstruction of the original image. Moreover, when δ in (4) has to be chosen

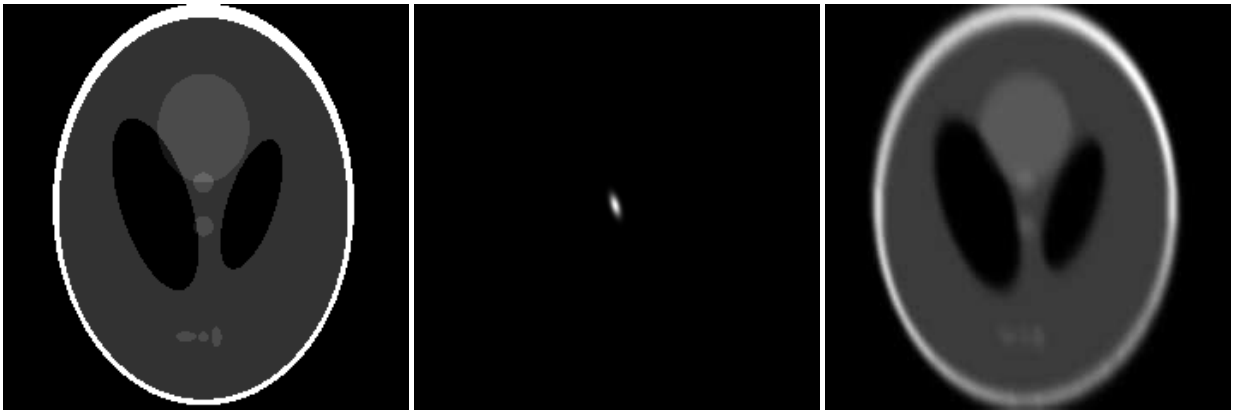

(a) (b) (c)

FIGURE 1 Phantom image: (a) true image (237 × 237 pixels), (b) PSF (237 × 237 pixels), (c) blurred and noise-free image (237 × 237 pixels).

large (enough), the AIT and MAIT methods are equivalent and produce reconstructions of the same quality. In this section, we set $\delta = \|\boldsymbol{\eta}\|$.

All the computations were carried out in Matlab R2018b with about 15 significant decimal digits on a Windows 10 laptop with an i7-8750H @2.20 GHz with 16 GB of RAM.

Phantom

We first consider Example 2 in [16], which discusses restoration of a phantom image. The exact image is blurred with a nonsymmetric Gaussian PSF from [26]; see Figure 1. Due to the nature of this image, we impose zero boundary conditions.

The authors of [16] pointed out that the AIT method may fail for this example when there is not enough noise in the available blur- and noise-contaminated image to be restored. They proposed a possible strategy to remedy this issue, namely to increase the value of ρ. We consider here two choices for the noise level δ and two choices for the parameter ρ, and compare the results. Thus, we let $\delta \in \{0.1\% \|\mathbf{b}\|, 1\% \|\mathbf{b}\|\}$ and $\rho \in \{10^{-3}, 10^{-2}\}$. We report the computed results in Table 1. We can observe that, for $\rho = 10^{-3}$ and $\delta = 0.1\% \|\mathbf{b}\|$, the AIT method provides very unsatisfactory results. As pointed out in [16], this behavior can be identified by observing the computed values of μ_k, which become very oscillatory for increasing k. In this case, i.e., when $\delta = 0.1\% \|\mathbf{b}\|$, we are able to "save" the AIT method by increasing the value of ρ, and obtain good reconstructions. On the other hand, when $\delta = 1\% \|\mathbf{b}\|$, the AIT and MAIT methods produce very similar results, independently of the choice of ρ. Finally, we observe that the MAIT method is able to produce satisfactory reconstructions for all noises level and values of ρ.

Figure 2 reports the behavior of the RRE versus the number of iterations for all cases considered. By visual inspection of these graphs, we can observe that the iterations with the MAIT method are terminated before the RRE grows when $\delta = 0.1\% \|\mathbf{b}\|$ and $\rho = 10^{-3}$. On the other hand, when AIT converges, the MAIT method behaves very similarly and, although the iterations stop earlier, the quality of the reconstructions is about the same; see Figs. 3 and 4.

We would like to point out that, in this case, the RRE obtained with MAIT for $\delta = 0.1\% \|\mathbf{b}\|$ is larger than the RRE obtained for $\delta = 1\% \|\mathbf{b}\|$. This is due to the fact that, when $\|\mathbf{b}\|$ is small, δ is quite small as well, and the chosen value of β tends to stop the iterations earlier than needed. This illustrates the fact that the MAIT method is not a regularization method. Nevertheless, we can observe that the SSIM for the computed reconstructions is larger for $\delta = 0.1\% \|\mathbf{b}\|$ than for $\delta = 1\% \|\mathbf{b}\|$.

Cameraman

Our second example considers the cameraman image. We blur the exact image with an average PSF; see Figure 5. Since the image is generic, we impose reflective boundary conditions. We first fix $\rho = 10^{-3}$. Two noise levels are considered, $\delta_1 = 0.1\% \|\mathbf{b}\|$ and $\delta_2 = 1\% \|\mathbf{b}\|$. Figure 6 displays the RRE at each iteration for both the AIT and MAIT methods for both noise levels. We can observe that when the noise level is small, the AIT method fails to converge. In this particular case, after the 18th iterations, some entries of the reconstructed solution become `NaN` and, thus, we cannot compute the RRE or visualize the reconstruction. The MAIT method produces an accurate reconstruction and the RRE stabilizes after very few iterations. When we increase the noise level to 1%, we note that the two methods are numerically equivalent and produce the same reconstruction. We would

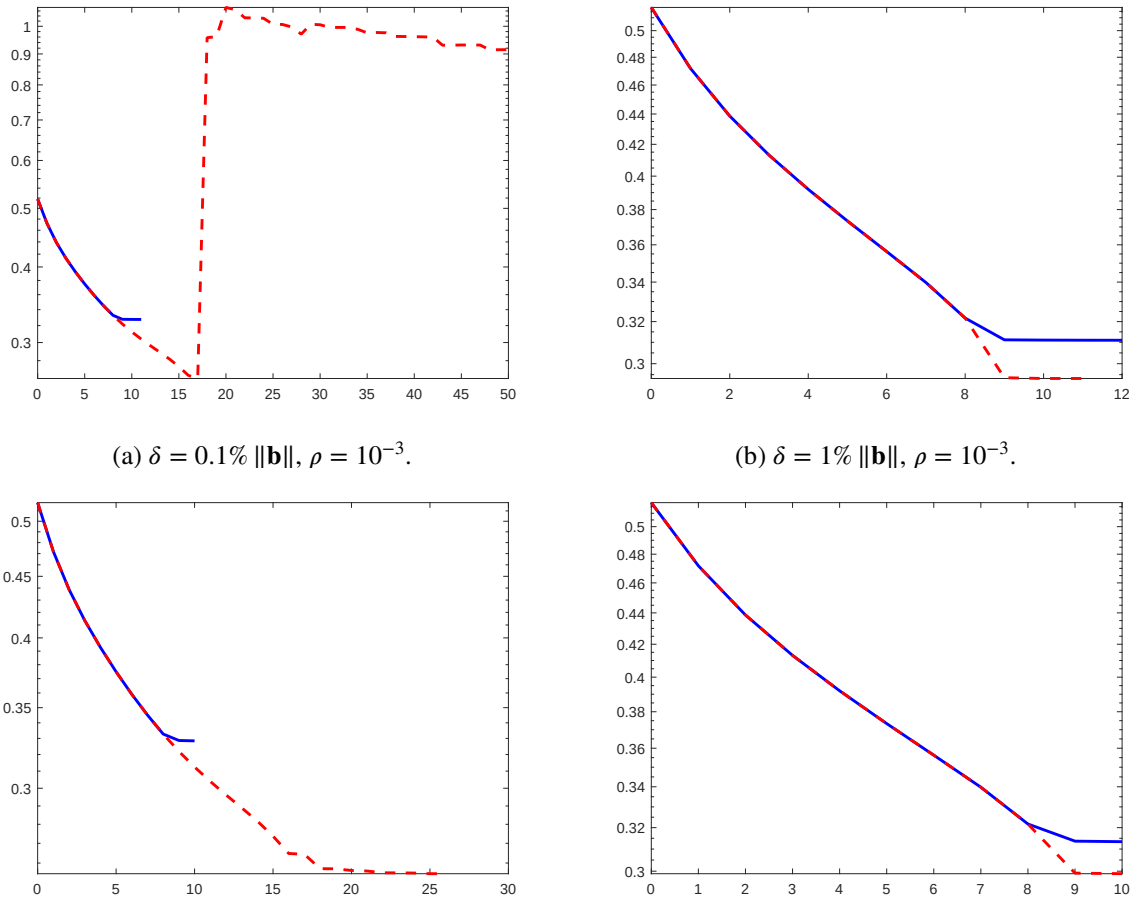

(a) $\delta = 0.1\% \, \|\mathbf{b}\|$, $\rho = 10^{-3}$.

(b) $\delta = 1\% \, \|\mathbf{b}\|$, $\rho = 10^{-3}$.

(c) $\delta = 0.1\% \, \|\mathbf{b}\|$, $\rho = 10^{-2}$.

(d) $\delta = 1\% \, \|\mathbf{b}\|$, $\rho = 10^{-2}$.

FIGURE 2 Phantom image: plot of the RRE against the iterations for different choices of δ and ρ, the red dashed curve is the RRE for the AIT method, while the blue solid curve is the RRE for MAIT method. We report below each figure the values of δ and ρ.

like to show that, in this case, increasing ρ does not allow the AIT method to converge when $\delta = \delta_1$. We now fix $\rho = 10^{-1}$ and consider the same noise levels as before. Figure 6 shows that also in this case the AIT method fails to converge when $\delta = \delta_1$. This illustrates that it is not possible to "save" the convergence of AIT by increasing the value of ρ. These considerations are confirmed by visual inspection of the reconstructions in Figure 7 and 8 and by the RRE and SSIM values reported in Table 1.

We would like to briefly discuss the effect of changing the parameter β in the MAIT algorithm. Consider the noise level $\delta_1 = 0.1\% \, \|\mathbf{b}\|$, run the MAIT algorithm for $\beta \in \{50, 100, 150, 200\}$, and plot the RRE against the iteration number for all cases. The results are reported in Figure 9. We observe that for $\beta = 50$, the MAIT and AIT methods perform the same. The MAIT method also converges for the other choices of β. The larger β-value, the earlier the iterations with the MAIT method are stopped. This is to be expected, since a large value of β implies that we do not "trust" the matrix C to be an accurate approximation of A, and therefore terminate the iteration earlier.

Finally, we would like to note that, in this particular case, since the PSF is quadrantally symmetric, the matrix A can be diagonalized by the discrete cosine transform. However, we do not exploit this property for uniformity and in order to show the generality of the proposed method.

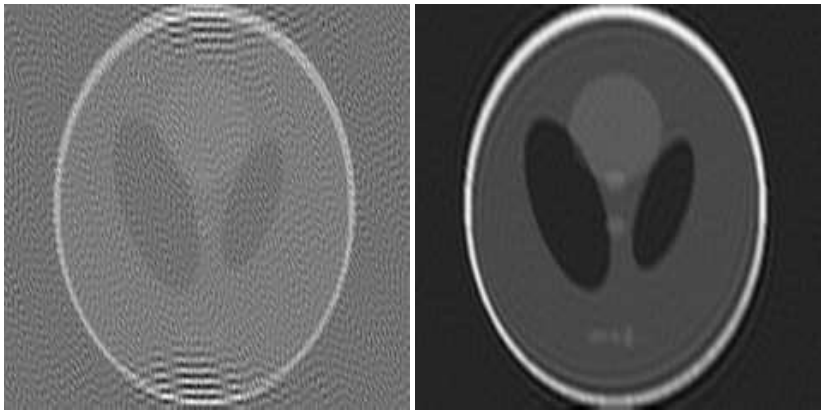

(a) AIT, $\delta = 0.1\% \, \|\mathbf{b}\|$ (b) AIT, $\delta = 1\% \, \|\mathbf{b}\|$

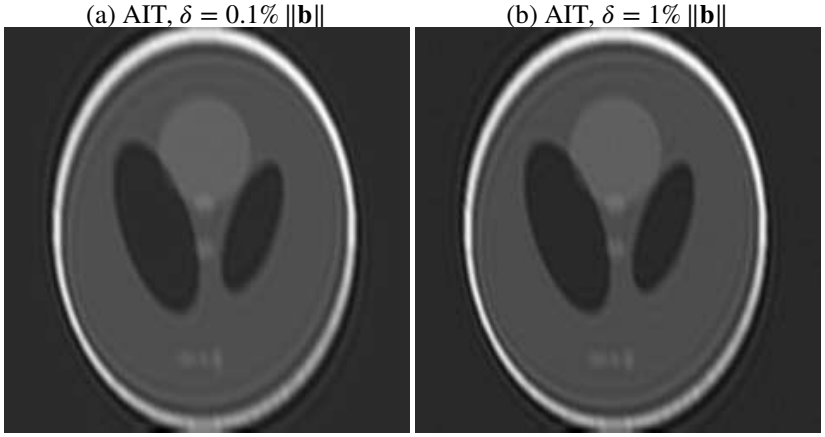

(c) MAIT, $\delta = 0.1\% \, \|\mathbf{b}\|$ (d) MAIT, $\delta = 1\% \, \|\mathbf{b}\|$

FIGURE 3 Phantom image reconstructions with $\rho = 10^{-3}$. We report below each figure the algorithm used for computing the reconstruction and the value of δ.

Clock

For our third example, we consider the clock image in Figure 10(a). We blur this image using the motion PSF in Figure 10(b). This yields the blurred (and noise-free image) in Figure 10(c). Just as in the previous example, we use two different noise levels: $\delta_1 = 0.1\% \, \|\mathbf{b}\|$ and $\delta_2 = 1\% \, \|\mathbf{b}\|$. Since the image is generic we use reflexive boundary conditions.

Figure 11 reports the evolution of the RRE throughout the iterations, and Table 1 displays the final values of the RRE and SSIM for both the AIT and MAIT methods and for both noise levels. We can observe that, like in the previous example, the AIT method fails to converge when the noise level is small, while the MAIT method is able to provide an accurate reconstruction in this situation. On the other hand, for larger noise levels, the AIT and MAIT methods are numerically equivalent and produce identical reconstructions. These observations are confirmed by visual inspection of the reconstructions in Figure 12.

Like in the previous example, also for this case the AIT method is not convergent for any value of ρ when $\delta = \delta_1$. Since the results are very similar as above, we do not consider other choices of ρ.

Grain

We describe the performance of the AIT and MAIT methods when applied to the grain image in Figure 13(a). We blur this image with the non-symmetric PSF shown in Figure 13(b). The blurred image so obtained is depicted in Figure 13(c). We use the noise levels $\delta = 0.1\% \, \|\mathbf{b}\|$ and $\delta = 1\% \, \|\mathbf{b}\|$, and compare the reconstructions obtained. Due to the nature of the considered image we impose reflexive boundary conditions.

Figure 14 and Table 1 report the evolution of the RRE and the final RRE and SSIM for the AIT and MAIT methods. The relative performance of these methods is similar as in the previous two examples. For $\delta = \delta_1$ the AIT method fails to converge, while the MAIT method stops after fewer than 15 iterations and produces a very satisfactory reconstruction; see Figure 15(c).

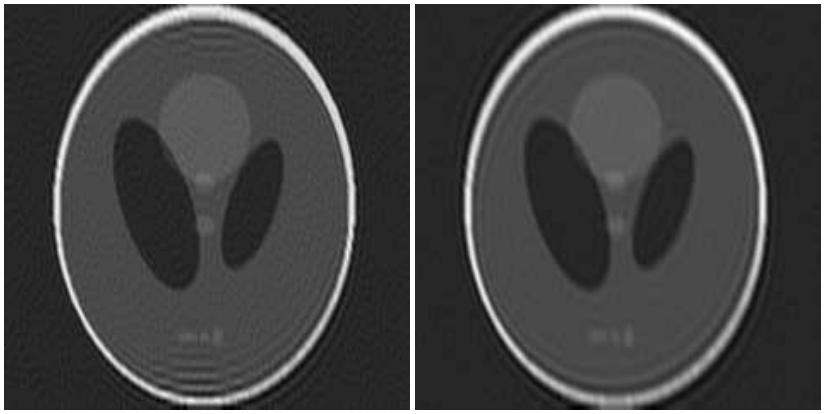

(a) AIT, $\delta = 0.1\% \, \|\mathbf{b}\|$ (b) AIT, $\delta = 1\% \, \|\mathbf{b}\|$

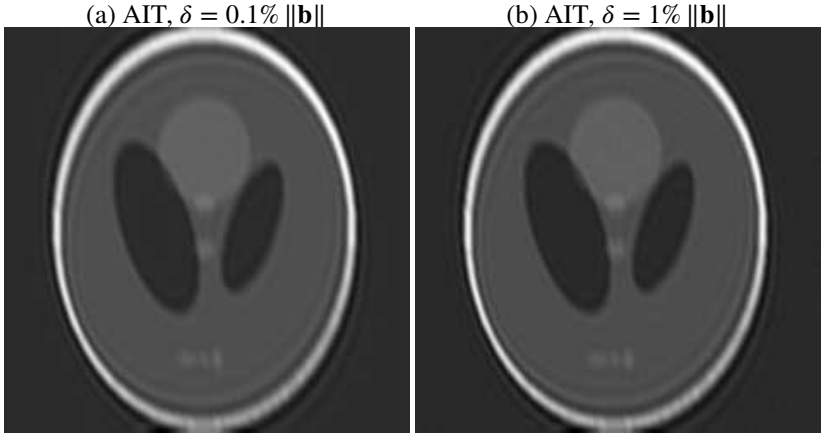

(c) MAIT, $\delta = 0.1\% \, \|\mathbf{b}\|$ (d) MAIT, $\delta = 1\% \, \|\mathbf{b}\|$

FIGURE 4 Phantom image reconstructions with $\rho = 10^{-2}$: We report below each figure the algorithm used for computing the reconstruction and the value of δ.

When we use a higher noise level, $\delta = \delta_2$, both methods converge and provide very similar reconstructions. These observations are confirmed by visual inspection of the reconstructions depicted in Figure 15.

Finally, we would like to stress that, like in the previous two cases, the AIT method does not converge for any choice of ρ, when $\delta = 0.1\% \, \|\mathbf{b}\|$. Since these results are very similar to the ones discussed above, we do not report the details.

4.1 | Nonstationary choice of β

As we discussed above, the choice of the parameter β is not crucial for the algorithm, however, it influences the quality of the reconstructed solution somewhat; see Figure 9. In particular, a large value of β may terminate the iterations too early; see the phantom example.

We outline a heuristic approach for improving the quality of the computed solution by replacing the fixed value of β used in the previous computations by a a nonstationary sequence of values of β. We will choose the sequence

$$\beta_k = \min\{(k-1)^2, \beta_{\max}\},$$

where $\beta_{\max}$ is the maximum value we would like β_k to attain. In our experiments, we set $\beta_{\max} = 150$. The intuition supporting this heuristic choice is that the AIT method starts to diverge only after some iterations have been carried out, but the very first iterations are stable. The increasing sequence of β_ks allows us to exploit properties of the AIT method during the first few iteration and in later iterations the method behaves like MAIT. This approach seeks to avoid that the iterations with the MAIT method terminate too early. However, this approach is heuristic and may fail in some situations. Finally, we would like to mention that the idea of using an increasing sequence of regularization parameter has previously been exploited in the iterated Tikhonov regularization method; see[27]. Algorithm 3 describes the nonstationary MAIT algorithm.

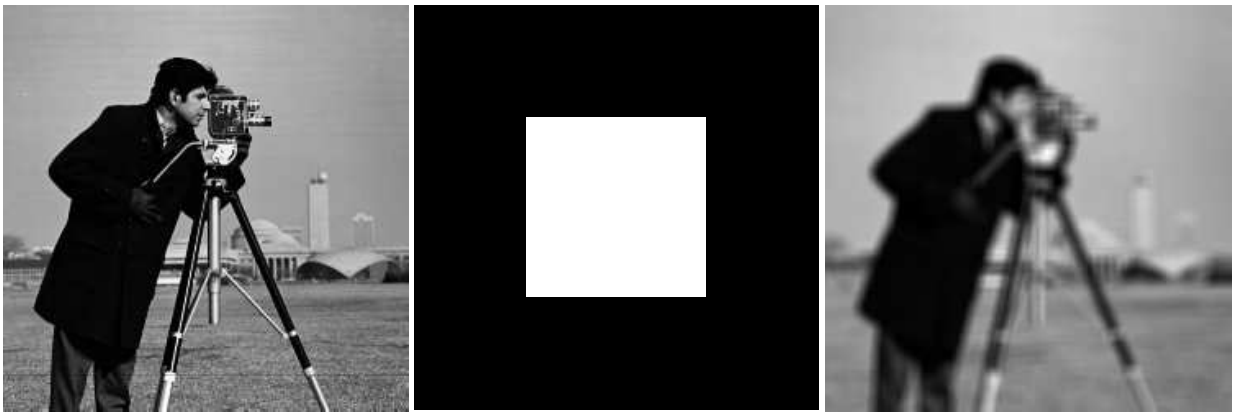

(a) (b) (c)

FIGURE 5 Cameraman image: (a) true image (248×248 pixels), (b) PSF (18×18 pixels), (c) blurred and noise-free image (248×248 pixels).

Algorithm 3 MAIT_{NS}

Let A and C satisfy Assumption 2 for given $0 < \rho < 1/2$ and $\beta_{\max} \geq 0$. Fix $q \in (2\rho, 1)$, let $\delta > 0$ satisfy (4), and let $\mathbf{x}_0$ be an initial approximation of $\mathbf{x}^\dagger$.

$\mathbf{r}_0 = \mathbf{b}^\delta - A\mathbf{x}_0$
$\tau = \frac{1+2\rho}{1-2\rho}$
for $k = 0, 1, \ldots$ **do**
  $\beta_k = \min\{(k-1)^2, \beta_{\max}\}$
  $t_0 = \min\left\{\frac{\delta}{\beta_k}, \frac{\beta_k}{\delta}\right\} + 1$
  $\tau_k = t_0 \dfrac{\|\mathbf{r}_k\|}{\delta + \beta_k}$
  $q_k = \max\{q, 2\rho + (1+\rho)/\tau_k\}$ Determine μ_k such that $\|\mathbf{r}_k - CC^T(CC^T + \mu_k I)^{-1}\mathbf{r}_k\| = q_k\|\mathbf{r}_k\|$
  $\mathbf{h}_k = C^T(CC^T + \mu_k)^{-1}\mathbf{r}_k$
  $\mathbf{x}_{k+1} = \mathbf{x}_k + \mathbf{h}_k$
  $\mathbf{r}_{k+1} = \mathbf{b}^\delta - A\mathbf{x}_{k+1}$
  if $\|\mathbf{r}_{k+1}\| \leq \tau\delta$ or $\|\mathbf{r}_{k+1}\| \leq \tau\dfrac{\delta + \beta_k}{t_0}$ **then**
    exit
  end if
end for

We apply the proposed nonstationary algorithm to all the previous examples. The results are reported in Table 1. The computed reconstructions are displayed in Figure 16. We can observe that the MAIT_{NS} method generally is able to provide more accurate reconstructions than both the MAIT and AIT methods for $\delta = 0.1\% \|\mathbf{b}\|$ and to determine reconstructions of the same quality as both the AIT and MAIT methods when $\delta = 1\% \|\mathbf{b}\|$. The only exception is the clock image, for which the MAIT_{NS} method fails to converge for $\delta = 0.1\% \|\mathbf{b}\|$. This behavior is due to the fact that for this image, the AIT method diverges very quickly (see Figure 11(a)) and the chosen sequence of β-values does not increase fast enough.

5 | CONCLUSIONS

This paper describes a modification of the preconditioned method proposed in [16]. The convergence analysis in [16] requires a very strong condition to hold. Our modified preconditioned method can be shown to converge, albeit in a weaker sense (see Theorem 3), under much weaker conditions. Moreover, we illustrate that under certain circumstances the method in [16] may

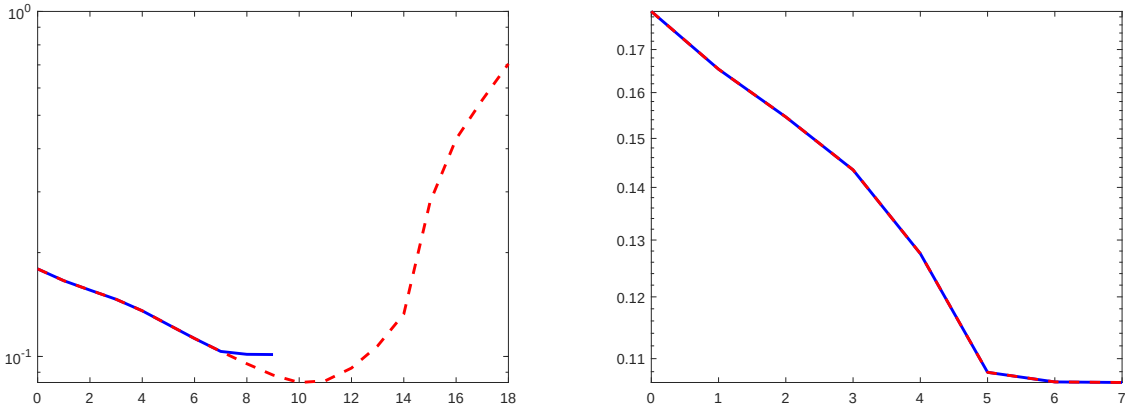

(a) $\delta = 0.1\% \, \|\mathbf{b}\|$, $\rho = 10^{-3}$

(b) $\delta = 1\% \, \|\mathbf{b}\|$, $\rho = 10^{-3}$

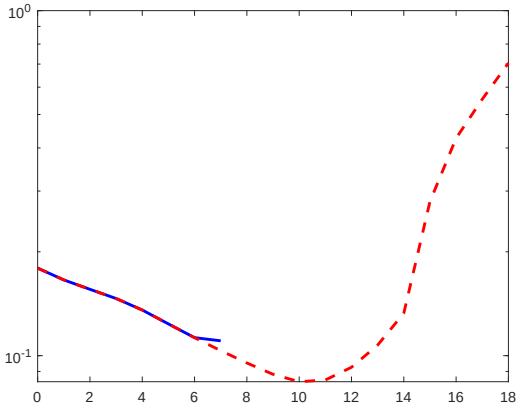

(c) $\delta = 0.1\% \, \|\mathbf{b}\|$, $\rho = 10^{-1}$

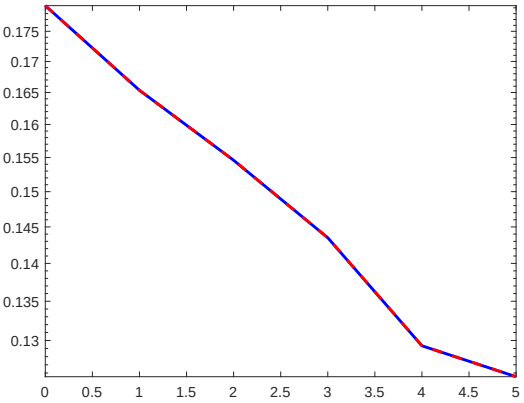

(d) $\delta = 1\% \, \|\mathbf{b}\|$, $\rho = 10^{-1}$

FIGURE 6 Cameraman image: plot of the RRE against the iterations for different choices of δ and ρ, the red dashed curve is the RRE for the AIT method, while the blue solid curve is the RRE for MAIT method. We report below each figure the values of δ and ρ.

fail to converge and produce unsatisfactory results, while our modification is able to provide accurate computed solutions. An extension of our modification to the iterative method discussed in [17] is a topic of future research.

ACKNOWLEDGMENTS

We would like to thank the referees for comments. A.B. and M.D. are members of the GNCS-INdAM group. The work of A.B. has been partially supported by the Young Researchers Project (Progetto Giovani Ricercatori) "Variational methods for the approximation of sparse data" of the GNCS-INdAM group. Moreover, A.B. research is partially supported by the Regione Autonoma della Sardegna research project "Algorithms and Models for Imaging Science [AMIS]" (RASSR57257, intervento finanziato con risorse FSC 2014-2020 - Patto per lo Sviluppo della Regione Sardegna). The work of L.R is supported in part by NSF grants DMS-1720259 and DMS-1729509. The work of W.Z. is supported by the China Scholarship Council (CSC No. 201806180081).

(a) AIT, $\delta = 0.1\% \, \|\mathbf{b}\|$ (b) AIT, $\delta = 1\% \, \|\mathbf{b}\|$

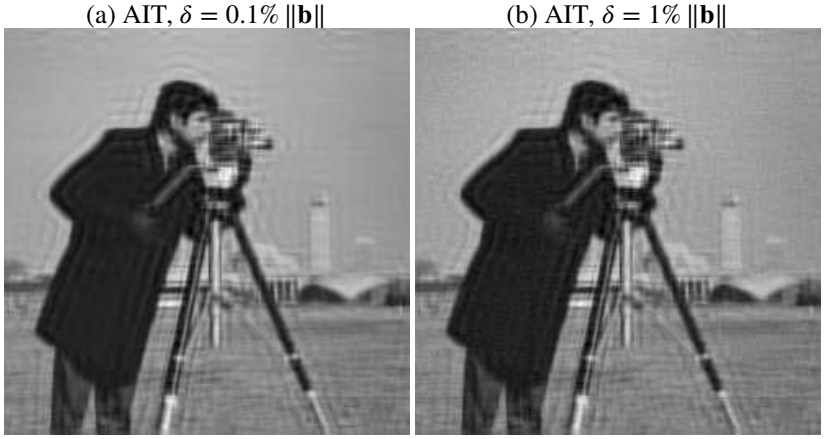

(c) MAIT, $\delta = 0.1\% \, \|\mathbf{b}\|$ (d) MAIT, $\delta = 1\% \, \|\mathbf{b}\|$

FIGURE 7 Cameraman image reconstructions with $\rho = 10^{-3}$. We report below each figure the algorithm used for computing the reconstruction and the value of δ.

References

1. Engl HW, Hanke M, and Neubauer A. Regularization of inverse problems. vol. 375. Springer Science & Business Media; 1996.

2. Hansen PC. Rank Deficient and Discrete Ill-Posed Problems: Numerical Aspects of Linear Inversion. SIAM, Philadelphia; 1998.

3. Fenu C, Reichel L, and Rodriguez G. GCV for Tikhonov regularization via global Golub–Kahan decomposition. Numerical Linear Algebra with Applications. 2016;**23**(3):467–484.

4. Kindermann S. Convergence analysis of minimization-based noise level-free parameter choice rules for linear ill-posed problems. Electron Trans Numer Anal. 2011;**38**:233–257.

5. Kindermann S, and Raik K. A simplified L-curve method as error estimator. Electronic Transactions on Numerical Analysis. 2020;**53**:217–238.

6. Gazzola S, Novati P, and Russo MR. Embedded techniques for choosing the parameter in Tikhonov regularization. Numerical Linear Algebra with Applications. 2014;**21**(6):796–812.

7. Bai ZZ, Buccini A, Hayami K, Reichel L, Yin JF, and Zheng N. Modulus-Based Method for Constrained Tikhonov Regularization. Journal of Computational and Applied Mathematics. 2017;**319**:1–13.

8. Calvetti D, Lewis BW, Reichel L, and Sgallari F. Tikhonov regularization with nonnegativity constraint. Electronic Transactions on Numerical Analysis. 2004;**18**:153–173.

(a) AIT, $\delta = 0.1\% \, \|\mathbf{b}\|$ (b) AIT, $\delta = 1\% \, \|\mathbf{b}\|$

(c) MAIT, $\delta = 0.1\% \, \|\mathbf{b}\|$ (d) MAIT, $\delta = 1\% \, \|\mathbf{b}\|$

FIGURE 8 Cameraman image reconstructions with $\rho = 10^{-1}$. We report below each figure the algorithm used for computing the reconstruction and the value of δ.

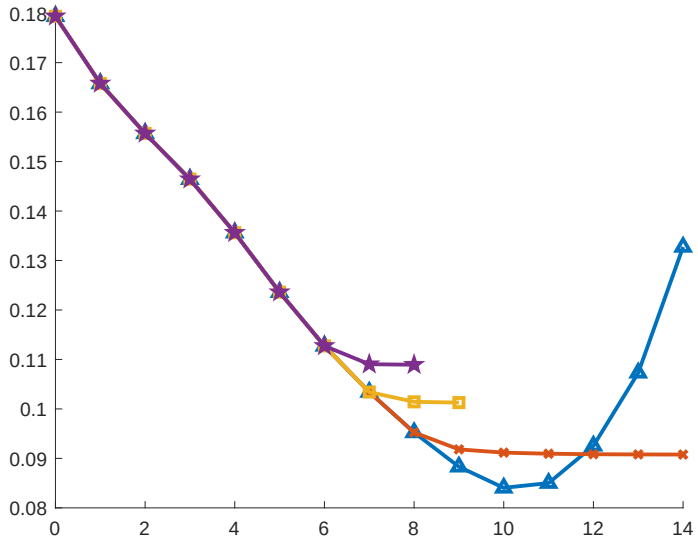

FIGURE 9 Cameraman image: plot of the RRE against the iterations for the MAIT method for different choices of β. The blue curve with triangles corresponds to $\beta = 50$, the red curve with crosses corresponds to $\beta = 100$, the yellow curve with squares corresponds to $\beta = 150$, and the purple curve with pentagrams corresponds to $\beta = 200$.

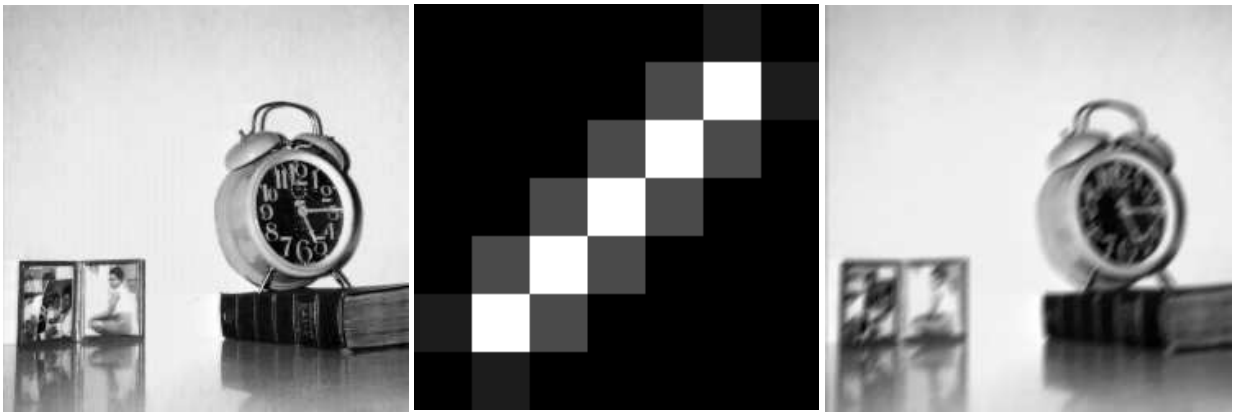

(a) (b) (c)

FIGURE 10 Clock image: (a) true image (248×248 pixels), (b) PSF (7×7 pixels), (c) blurred and noise-free image (248×248 pixels).

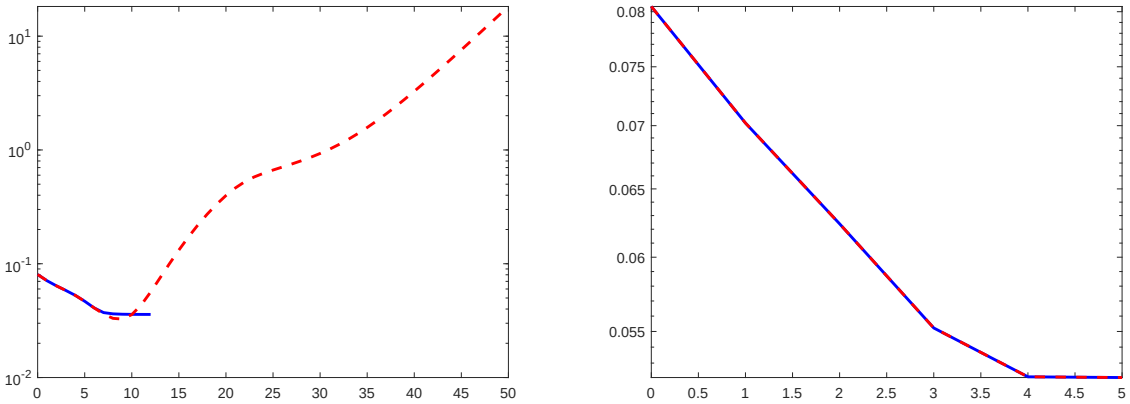

(a) $\delta = 0.1\%\ \|\mathbf{b}\|$, $\rho = 10^{-3}$ (b) $\delta = 1\%\ \|\mathbf{b}\|$, $\rho = 10^{-3}$

FIGURE 11 Clock image: plot of the RRE against the iterations for different choices of δ, the red dashed curve is the RRE for the AIT method, while the blue solid curve is the RRE for MAIT method. We report below each figure the values of δ and ρ.

9. Nagy JG, and Strakos Z. Enforcing nonnegativity in image reconstruction algorithms. In: International Symposium on Optical Science and Technology. International Society for Optics and Photonics; 2000. p. 182–190.

10. Gazzola S, and Wiaux Y. Fast nonnegative least squares through flexible Krylov subspaces. SIAM Journal on Scientific Computing. 2017;**39**(2):A655–A679.

11. Buccini A, Pasha M, and Reichel L. Generalized singular value decomposition with iterated Tikhonov regularization. Journal of Computational and Applied Mathematics. 2020;**373**:112276.

12. Donatelli M, and Reichel L. Square smoothing regularization matrices with accurate boundary conditions. Journal of Computational and Applied Mathematics. 2014;**272**:334–349.

13. Klann E, and Ramlau R. Regularization by fractional filter methods and data smoothing. Inverse Problems. 2008;**24**(2):025018.

14. Hochstenbach ME, and Reichel L. Fractional Tikhonov regularization for linear discrete ill-posed problems. BIT Numerical Mathematics. 2011;**51**(1):197–215.

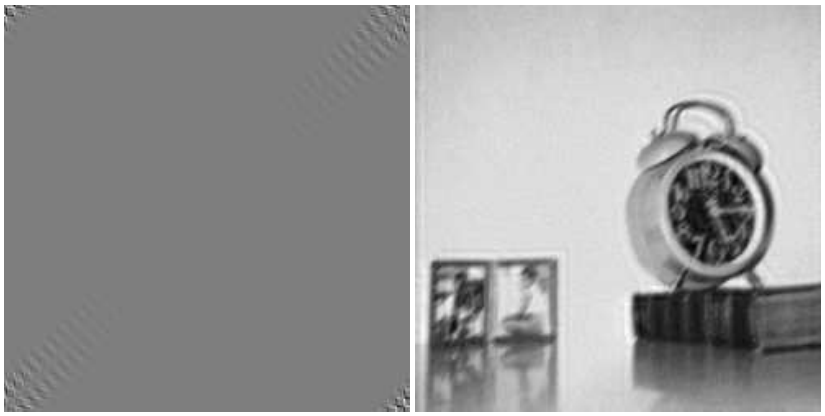

(a) AIT, $\delta = 0.1\% \, \|\mathbf{b}\|$ (b) AIT, $\delta = 1\% \, \|\mathbf{b}\|$

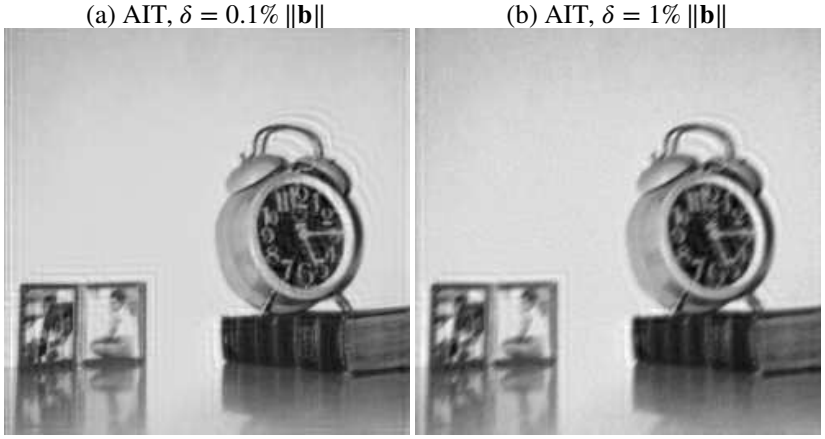

(c) MAIT, $\delta = 0.1\% \, \|\mathbf{b}\|$ (d) MAIT, $\delta = 1\% \, \|\mathbf{b}\|$

FIGURE 12 Clock image reconstruction with $\rho = 10^{-3}$. We report below each figure the algorithm used for computing the reconstruction and the value of δ.

15. Hanke M, and Groetsch CW. Nonstationary iterated Tikhonov regularization. Journal of Optimization Theory and Applications. 1998;**98**(1):37–53.

16. Donatelli M, and Hanke M. Fast nonstationary preconditioned iterative methods for ill-posed problems, with application to image deblurring. Inverse Problems. 2013;**29**(9):095008.

17. Buccini A. Regularizing preconditioners by non-stationary iterated Tikhonov with general penalty term. Applied Numerical Mathematics. 2017;**116**:64–81.

18. Bianchi D, Buccini A, Donatelli M, and Serra-Capizzano S. Iterated fractional Tikhonov regularization. Inverse Problems. 2015;**31**(5):055005.

19. Buccini A, Donatelli M, and Reichel L. Iterated Tikhonov regularization with a general penalty term. Numerical Linear Algebra with Applications. 2017;**24**(4):e2089.

20. Buccini A, Park Y, and Reichel L. Numerical aspects of the nonstationary modified linearized Bregman algorithm. Applied Mathematics and Computation. 2018;**337**:386–398.

21. Buccini A, and Donatelli M. A multigrid frame based method for image deblurring. Electronic Transactions on Numerical Analysis. 2020;**53**:283–312.

22. Bianchi D, and Buccini A. Generalized structure preserving preconditioners for frame-based image deblurring. Mathematics. 2020;**8**(4):468.

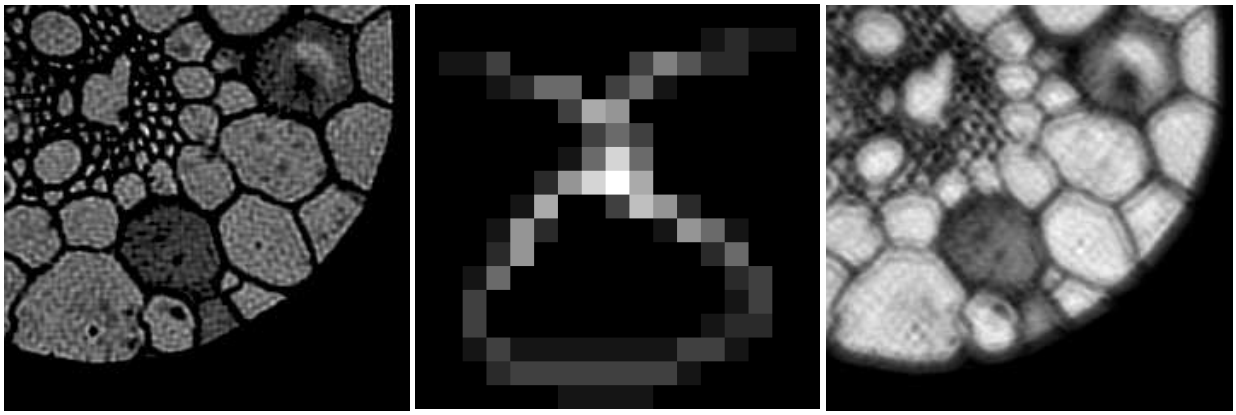

(a) (b) (c)

FIGURE 13 Grain image: (a) true image (238×238 pixels), (b) PSF (17×17 pixels), (c) blurred and noise-free image (238×238 pixels).

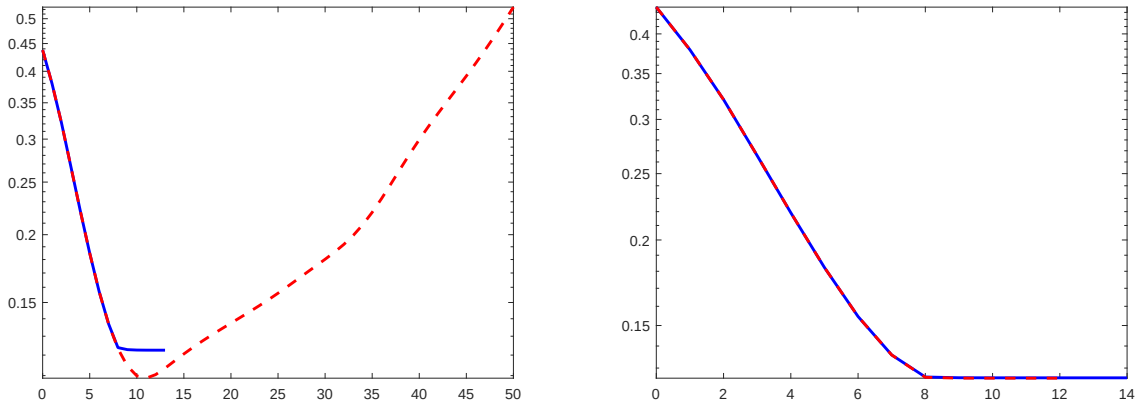

(a) $\delta = 0.1\%\ \|\mathbf{b}\|$, $\rho = 10^{-3}$ (b) $\delta = 1\%\ \|\mathbf{b}\|$, $\rho = 10^{-3}$

FIGURE 14 Grain image: plot of the RRE against the iterations for different choices of δ, the red dashed curve is the RRE for the AIT method, while the blue solid curve is the RRE for MAIT method. We report below each figure the values of δ and ρ.

23. Bianchi D, Buccini A, and Donatelli M. Structure preserving preconditioning for frame-based image deblurring. In: Computational Methods for Inverse Problems in Imaging. Springer, Cham; 2019. p. 33–49.

24. Hansen PC, Nagy JG, and O'Leary DP. Deblurring Images: Matrices, Spectra, and Filtering. SIAM, Philadelphia; 2006.

25. Wang Z, Bovik AC, Sheikh HR, and Simoncelli EP. Image quality assessment: from error visibility to structural similarity. IEEE Transactions on Image Processing. 2004;**13**(4):600–612.

26. Berisha S, and Nagy JG. 2012. *Iterative Methods for Image Restoration*. . Department of Mathematics and Computer Science, Emory University. http://www.mathcs.emory.edu/~nagy/RestoreTools/IR.pdf.

27. Donatelli M. On nondecreasing sequences of regularization parameters for nonstationary iterated Tikhonov. Numerical Algorithms. 2012;**60**(4):651–668.

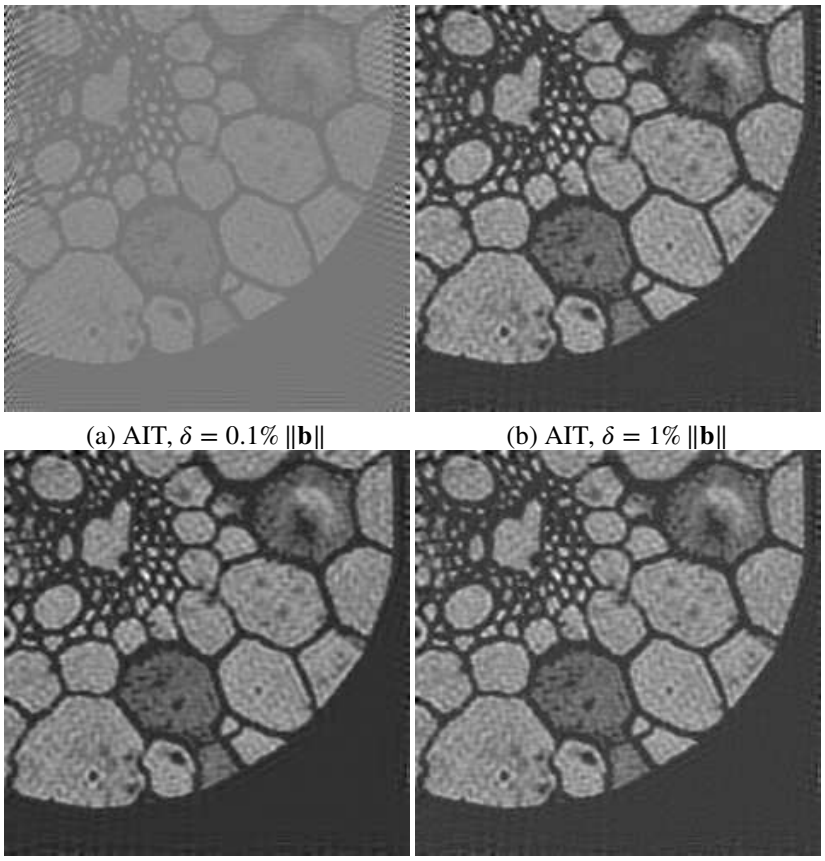

(a) AIT, $\delta = 0.1\% \, \|\mathbf{b}\|$ (b) AIT, $\delta = 1\% \, \|\mathbf{b}\|$

(c) MAIT, $\delta = 0.1\% \, \|\mathbf{b}\|$ (d) MAIT, $\delta = 1\% \, \|\mathbf{b}\|$

FIGURE 15 Grain image reconstruction with $\rho = 10^{-3}$. We report below each figure the algorithm used for computing the reconstruction and the value of δ.

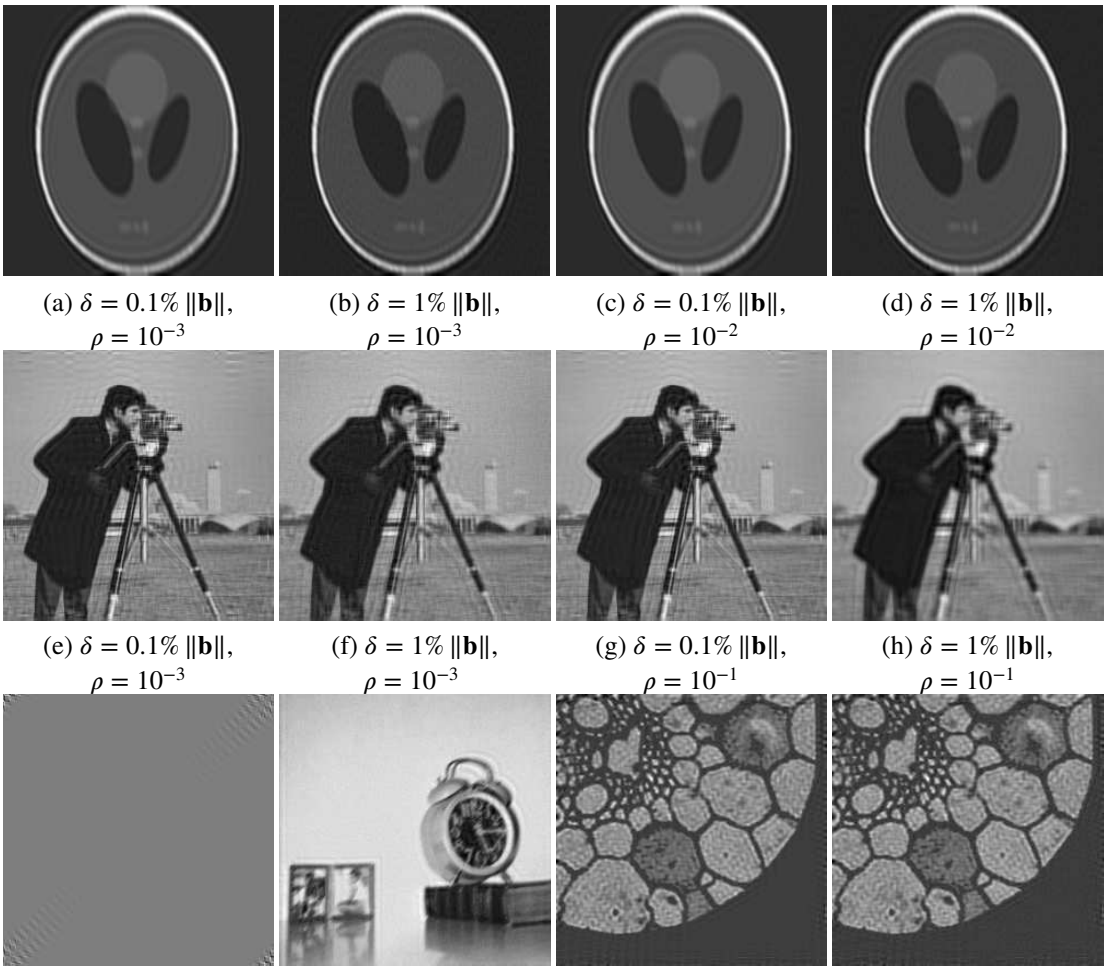

(a) $\delta = 0.1\% \, \|\mathbf{b}\|$, $\rho = 10^{-3}$ (b) $\delta = 1\% \, \|\mathbf{b}\|$, $\rho = 10^{-3}$ (c) $\delta = 0.1\% \, \|\mathbf{b}\|$, $\rho = 10^{-2}$ (d) $\delta = 1\% \, \|\mathbf{b}\|$, $\rho = 10^{-2}$

(e) $\delta = 0.1\% \, \|\mathbf{b}\|$, $\rho = 10^{-3}$ (f) $\delta = 1\% \, \|\mathbf{b}\|$, $\rho = 10^{-3}$ (g) $\delta = 0.1\% \, \|\mathbf{b}\|$, $\rho = 10^{-1}$ (h) $\delta = 1\% \, \|\mathbf{b}\|$, $\rho = 10^{-1}$

(i) $\delta = 0.1\% \, \|\mathbf{b}\|$, $\rho = 10^{-3}$ (j) $\delta = 1\% \, \|\mathbf{b}\|$, $\rho = 10^{-3}$ (k) $\delta = 0.1\% \, \|\mathbf{b}\|$, $\rho = 10^{-3}$ (l) $\delta = 1\% \, \|\mathbf{b}\|$, $\rho = 10^{-3}$

FIGURE 16 Reconstructions obtained with the MAIT_{NS} method for all considered examples. Below each figure we report the values of δ and ρ. Panels (a)-(d) are referred to the Phantom image, panels (e)-(h) are referred to the Cameraman image, panels (i) and (j) are referred to the Clock image, and panels (k) and (l) are referred to the Grain image.

TABLE 1 Comparison of the RRE and SSIM obtained by AIT, MAIT, and MAIT_{NS} in the considered examples.

Example	ρ	Noise Level	Method	RRE	SSIM
Phantom	10^{-3}	0.1%	AIT	0.91481	0.10378
			MAIT	0.32756	0.82184
			MAIT_{NS}	0.31245	0.83211
		1%	AIT	0.29326	0.79453
			MAIT	0.31098	0.81840
			MAIT_{NS}	0.29326	0.79453
	10^{-2}	0.1%	AIT	0.25475	0.72261
			MAIT	0.32847	0.82137
			MAIT_{NS}	0.31245	0.83211
		1%	AIT	0.29888	0.81120
			MAIT	0.31341	0.81808
			MAIT_{NS}	0.29888	0.81120
Cameraman	10^{-3}	0.1%	AIT	−−	−−
			MAIT	0.10128	0.79081
			MAIT_{NS}	0.086838	0.79514
		1%	AIT	0.10649	0.70911
			MAIT	0.10649	0.70911
			MAIT_{NS}	0.10637	0.70927
	10^{-1}	0.1%	AIT	−−	−−
			MAIT	0.11041	0.77641
			MAIT_{NS}	0.090613	0.79959
		1%	AIT	0.12544	0.73317
			MAIT	0.12544	0.73317
			MAIT_{NS}	0.12555	0.73289
Clock	10^{-3}	0.1%	AIT	18.231	0.017874
			MAIT	0.035864	0.92097
			MAIT_{NS}	18.174	0.017898
		1%	AIT	0.052109	0.84054
			MAIT	0.052109	0.84054
			MAIT_{NS}	0.052109	0.84054
Grain	10^{-3}	0.1%	AIT	0.52519	0.73557
			MAIT	0.12254	0.87857
			MAIT_{NS}	0.10988	0.89684
		1%	AIT	0.12565	0.84422
			MAIT	0.12579	0.84460
			MAIT_{NS}	0.12565	0.84422